A Four-Coordinate Pr^{4+} Imidophosphorane Complex

Andrew C. Boggiano,[a] Sabyasachi Roy Chowdhury,[b] Michael D. Roy,[a] Maximilian G. Bernbeck,[a] Samuel M. Greer,[c] Bess Vlaisavljevich,[b]* and Henry S. La Pierre[a][d]*

[a] Dr. A. C. Boggiano, Dr. M. D. Roy, Dr. M. G. Bernbeck, Prof. H. S. La Pierre
School of Chemistry & Biochemistry
Georgia Institute of Technology
Atlanta, GA 30332-0400 (USA)
E-mail: hsl@gatech.edu

[b] Dr. S. Roy Chowdhury, Prof. B. Vlaisavljevich
Department of Chemistry
University of South Dakota
Vermillion, SD 57069 (USA)
E-mail: Bess.Vlaisavljevich@usd.edu

[c] Dr. S. M. Greer
Chemistry Division
Los Alamos National Laboratory
Los Alamos, NM 87545 (USA)

[d] Prof. H. S. La Pierre
Nuclear and Radiological Engineering and Medical Physics Program, School of Mechanical Engineering
Georgia Institute of Technology
Atlanta, GA 30332-0400 (USA)

Supporting information for this article is given via a link at the end of the document.

Abstract: The imidophosphorane ligand, $[NP^tBu_3]^-$ (^{t}Bu = *tert*-butyl), enables isolation of a pseudo-tetrahedral, tetravalent praseodymium complex $[Pr^{4+}(NP^tBu_3)_4]$, **1-Pr**, which is characterized by a suite of physical characterization methods including single-crystal X-ray diffraction, electron paramagnetic resonance, and L_3-edge X-ray near-edge spectroscopies. Variable-temperature direct-current magnetic susceptibility data, supported by multiconfigurational quantum chemical calculations, demonstrate that the electronic structure diverges from the isoelectronic Ce^{3+} analogue due to increased crystal field. The four-coordinate environment around Pr^{4+} in **1-Pr**, which is unparalleled in reported extended solid systems, provides a unique opportunity to study the interplay between crystal field splitting and spin-orbit coupling in a molecular tetravalent lanthanide within a pseudo-tetrahedral coordination geometry.

An imidophosphorane ligand framework provided one of the first structurally authenticated examples of molecular Tb^{4+},[1] and the *in situ* characterization of Pr^{4+}.[2] The tetravalent oxidation state in molecular lanthanide (Ln) complexes has been documented in Tb[1, 3] and Pr,[2, 4] but remains largely confined to examples of Ce^{4+}.[5] Despite the similar thermodynamic accessibility of Pr^{4+} and Tb^{4+},[5a] multiple ligand systems which support isolable Tb^{4+} complexes yield fleeting Pr^{4+} complexes, precluding thorough physical characterization.[2, 3d, 4b] The open-shell electronic configuration of Pr^{4+}, in contrast to $4f^0$ Ce^{4+} systems, provides unique opportunities in the context of quantum information science and molecular magnetism.[4a, 4c, 6] We recently established[6-7] the intermediate coupling regime in extended solids containing Pr^{4+} units in near-octahedral oxide coordination environments, highlighting the consequences of the similar magnitude of crystal-field and spin-orbit coupling (SOC) effects on the electronic structure. Herein, we describe a rare example of an isolable molecular complex of Pr^{4+}, $[Pr^{4+}(NP^tBu_3)_4]$ (**1-Pr**, where ^{t}Bu = *tert*-butyl), which has been structurally characterized by single-crystal X-ray diffraction (SC-XRD), and further studied by a suite of physical methods, including L_3-edge X-ray near-edge absorption spectroscopy (XANES) and SQUID magnetometry (SQUID = superconducting quantum interference device). Magnetic data and electron paramagnetic resonance (EPR) spectroscopy, supported by second-order multireference methods, demonstrate divergence between the electronic structures of the isoelectronic ($4f^1$) Pr^{4+} and Ce^{3+} complexes.

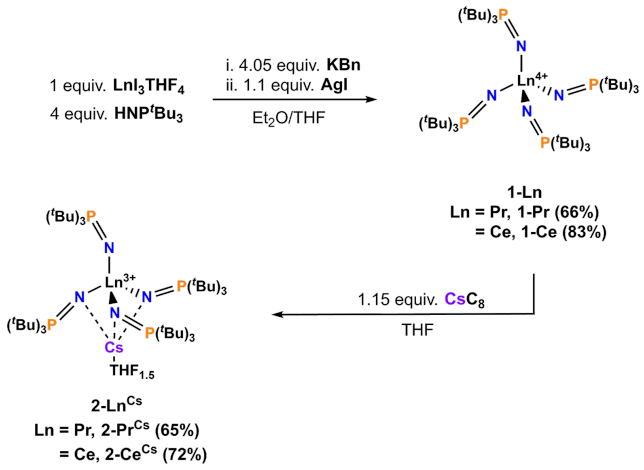

Scheme 1. Synthetic overview.

1-Pr and $[Ce^{4+}(NP^tBu_3)_4]$ (**1-Ce**), are both synthesized in one-pot, two-step reactions, consisting of a three-day reaction between $[LnI_3(THF)_4]$ (Ln = Ce, Pr), HNP^tBu_3, and benzyl potassium (KBn), followed by the addition of finely ground AgI (Scheme 1). Transmetallation of the $[NP^tBu_3]^{1-}$ via the sequential addition of HNP^tBu_3 and KBn was employed due to the poor solubility of $K[NP^tBu_3]$. An *in situ* oxidation was determined to be key for the isolation of monomeric species of tetravalent complexes **1-Pr** and **1-Ce**, as metathesis between $LnI_3(THF)_4$,

KBn, and HNP^{t}Bu$_3$, without sequential addition of AgI, did not cleanly afford [KLn^{3+}(NP^{t}Bu$_3$)$_4$]. The trivalent complexes are isolated as THF adducts of the Cs salts, ([Cs(THF$_x$)Ln^{3+}(NP^{t}Bu$_3$)$_4$], Ln = Pr, **2-Pr^{Cs}**, Ln = Ce, **2-Ce^{Cs}**; x = 1.5 after subjection to vacuum, x = 2 in single-crystal X-ray diffraction (SC-XRD) structures) via reduction of **1-Ln** with CsC_8 in THF. Cesium enabled isolation of well-defined single-crystal materials for structural analysis, as initial results of K^+ supported complexes prepared via KC_8 reduction of **1-Ln** provided crystals poorly suited for SC-XRD structural determination.

1-Pr is remarkably thermally robust, with no detectable degradation observed via $^{31}P\{^1H\}$ NMR spectroscopy after 72 h in a C_6D_6 solution at ambient temperature (~25 °C) inside a glovebox. After storage of the solution for 8 days, a resonance around 300 ppm (ostensibly a Pr^{3+} degradation product) is observed that integrates to a ratio of 0.1:1 ("Pr^{3+}":**1-Pr**). Mazzanti and co-workers report degradation of [Pr^{4+}(OSiPh$_3$)$_4$(MeCN)$_2$] (MeCN = acetonitrile) by 60% in toluene after 24 h (quantified by UV-Vis),[4b] however, by replacing one MeCN with triphenylphosphine oxide (OPPh$_3$), only 20% of [Pr^{4+}(OSiPh$_3$)$_4$(OPPh$_3$)(MeCN)] degrades in 24 h.[4a] Further improvement (43% degradation after 7 d) was recently reported by Zheng and co-workers, by replacing both MeCN molecules in [Pr^{4+}(OSiPh$_3$)$_4$(MeCN)$_2$] with a substituted bipyridine chelate.[4c] The thermal stability of **1-Pr** is in stark contrast to that of previously reported[2] [Pr^{4+}(N=P(1,2-di-^{t}Bu-ethylenediamide)(diethylamide))$_4$] (**1-Pr***), which has limited thermal stability and precluded its isolation as a pure solid.

1-Pr and **2-Pr^{Cs}** were structurally characterized by SC-XRD (Fig. 1). The average Pr^{4+}–N distance in **1-Pr** is 2.179(3) Å, compared to the average Pr^{3+}–N distance of 2.329(14) Å in **2-Pr^{Cs}**, consistent with the 0.14 Å difference in Shannon ionic radii between Pr^{4+} and Pr^{3+}.[8] **1-Pr** is pseudo-tetrahedral , with an average N–Pr^{4+}–N angle of 109.5(21) Å, and τ_4 index[9] of 0.97, indicating near-tetrahedral coordination geometry (Table S7). The average Ce^{4+}–N distance in **1-Ce** (2.176(4) Å) is statistically equivalent from that of **1-Pr**, consistent with the similar Shannon ionic radii of the neighboring lanthanides (0.87 Å for Ce^{4+} vs 0.85 Å for Pr^{4+}).[8] The trivalent complexes also have statistically equivalent structural parameters in line with the small changes in ionic radii; **2-Ce^{Cs}** has an average Ln^{3+}–N distance of 2.345(13) Å vs. 2.329(14) Å in **2-Pr^{Cs}**.

Electronic absorption spectroscopy (ultraviolet-visible-near-infrared, UV-vis-NIR) complements the structural data in validating oxidation state assignments. For the Pr complexes, the UV-vis-NIR spectra are particularly diagnostic, as **2-Pr^{Cs}** is practically transparent in the visible region, save the exceptionally weak ($\varepsilon \leq 10$ $M^{-1}cm^{-1}$) f-f transitions (Fig. S16). In contrast, the spectrum of **1-Pr** exhibits a strong, broad absorption (~400-1500 nm), with λ_{max} = 550 nm (ε = 8000 M^{-1} cm^{-1}), as well as a secondary feature at 299 nm (ε = 3600 M^{-1} cm^{-1}, Fig. S14, S15), resembling the spectrum of **1-Pr***.[2] The excitations were determined to be ligand-to-metal charge-transfer (LMCT) bands, from N 2p to Pr 4f orbitals, and were assigned from the spin-orbit states computed via state-interaction of restricted active space self-consistent field calculations[10] with an active space including Pr 4f, 5d, and ligand N 2p orbitals (Fig. S37, S38). The spectrum of **2-Ce^{Cs}** is consistent with reported examples for Ce^{3+} imidophosphorane complexes, with a 4f-5d transition observed at 375 nm (ε = 1300 $M^{-1}cm^{-1}$, Fig. S18).[11] The 4f-5d transition of **2-Ce^{Cs}** (λ_{max} = 375 nm, 26,700 cm^{-1}) is similar to previously reported complexes (Fig. S18).[11-12] Notably, the 4f-5d transition energy is consistent with the extended multistate complete active space second-order perturbation theory (XMS-CASPT2)[13] computed spin-free energy gap calculated between the 4f and 5d orbitals of **2-Ce^{Cs}** (~28,000 cm^{-1}, *vide infra*). The spectrum of **1-Ce** is also consistent with similar reported complexes,[11b, 11c, 12] featuring a broad LMCT feature with λ_{max} = 371 nm (ε = 15000 cm^{-1}, Fig. S17).

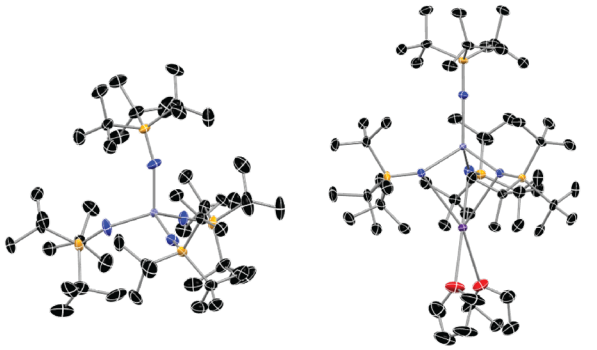

1-Pr | **2-Pr^{Cs}**

Avg. *d*(Pr^{4+}–N) = 2.179(3) Å | Avg. *d*(Pr^{3+}–N) = 2.329(14) Å
Avg. *d*(Ce^{4+}–N) = 2.176(4) Å | Avg. *d*(Ce^{3+}–N) = 2.345(13) Å

Figure 1. SC-XRD determined molecular structures of 1-Pr and 2-Pr^{Cs}. Thermal ellipsoids displayed at 50% probability. Average nitrogen-metal bond lengths displayed below with comparison to isotypic Ce congeners, 1-Ce and 2-Ce^{Cs}. Legend: Purple = Cs, Lilac = Pr, Orange = P, Red = O, Blue = N, Black = C. Ligand disorder and H atoms omitted for clarity.

1-Pr was characterized by L_3-edge X-ray near-edge spectroscopy (XANES), which probes the Ln $2p_{3/2}\rightarrow 5d$ core electron excitation. **1-Pr** exhibits a white line "doublet" feature that is characteristic of tetravalent lanthanides (Fig. 2A).[14] The spectrum of **1-Pr** is best modeled using three pseudo-Voigt functions, similar to the previously reported[11b, 11c] L_3-edge spectra of Ce^{4+} imidophosphorane complexes, including **1-Ce** (Fig. S22). The origin of multiple features is due to differing final states, one consisting of a ligand hole (<u>L</u>) and formal Ln^{3+} configuration, denoted as $4f^{n+1}\underline{L}5d^1$, and a higher energy feature associated with a formally tetravalent metal oxidation state ($4f^n5d^1$).[14a, 14c, 15] The ratio of the integrated area of fitted peaks is denoted as $A^{3+}/(A^{3+}+A^{4+})$, where A^{n+} is the integrated area corresponding to the peaks attributed to the Ln^{n+} final state configuration. For **1-Pr**, $A^{3+}/(A^{3+}+A^{4+})$ is calculated to be 0.73(5), with a value of 0.63(5) for **1-Ce** (Table S1). The similarity between **1-Pr** and **1-Ce** is consistent with studies of LnO_2 (Ln = Ce, Pr, Tb),[14a, 16] where Ce and Pr exhibit similar $A^{3+}/(A^{3+}+A^{4+})$ values and is indicative, in context of this model, of a similar degree Ln 4f/N 2p mixing in **1-Pr** and **1-Ce**. The previously reported[1] L_3-edge XANES spectrum of the related Tb^{4+} imidophosphorane complex, [Tb^{4+}(N=P(1,2-di-^{t}Bu-ethylenediamide)(diethylamide))$_4$] (**1-Tb***), contrasts **1-Ce** and **1-Pr**, and is satisfactorily modeled with only two peaks, with a lower $A^{3+}/(A^{3+}+A^{4+})$ value of 0.39(4). The trends observed between **1-Ce**, **1-Pr**, and **1-Tb*** are consistent with those observed for the LnO_2 series.[14a, 14b]

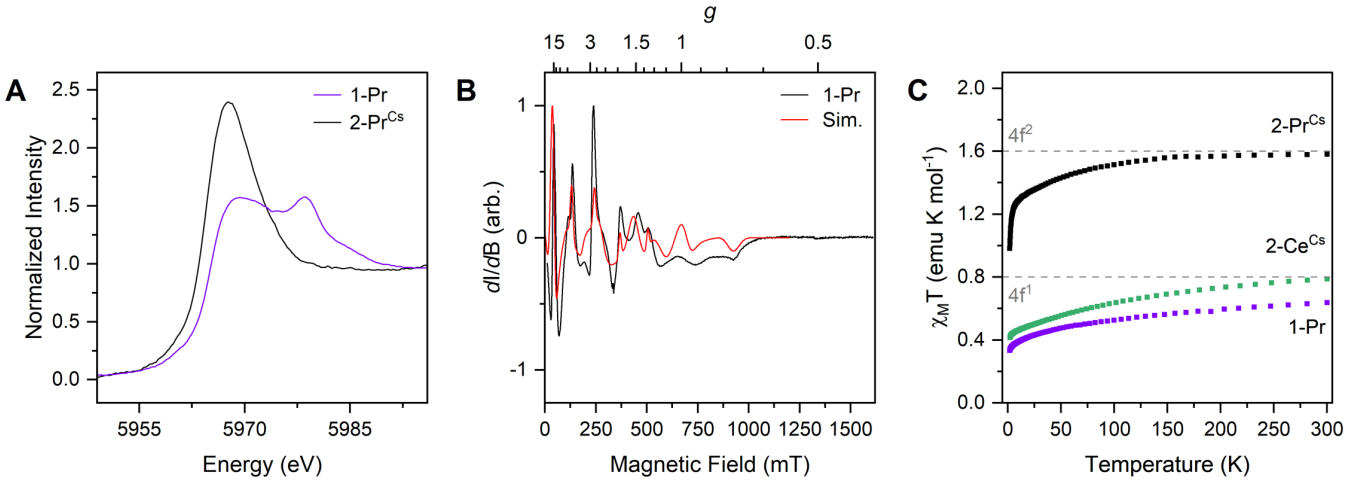

Figure 2. (A) Transmission L_3-edge XANES spectra of **1-Pr** and **2-Pr^{Cs}**. (B) X-band EPR spectrum of **1-Pr** in a 2-methyl-THF glass at 5 K. (C) χ_MT vs. temperature for **1-Pr**, **2-Pr^{Cs}**, and **2-Ce^{Cs}** under DC field of 1 T. Dotted lines represent calculated χ_MT values for $4f^1$ (0.80 emu K mol^{-1}) and $4f^2$ (1.6 emu K mol^{-1}) configurations.

Electron paramagnetic resonance (EPR) spectroscopy was performed on the isoelectronic $4f^1$ compounds, **1-Pr** and **2-Ce^{Cs}**. The X-band spectrum of **1-Pr** at 5 K in a 2-methyl-THF glass exhibits a spectrum (Fig. 2B) similar to the previously reported, *in situ* characterization of **1-Pr***.[2] The spectrum is complicated by strong hyperfine coupling to the 100% abundant ^{141}Pr nucleus (I = 5/2), and significant g-anisotropy.[6, 17] Similar to previous studies, spectral simulation was used to show that the complex spectrum of **1-Pr** can be qualitatively reproduced with spin Hamiltonian parameters consistent with those expected for a Pr^{4+} ion. The simulation of the experimental spectrum of **1-Pr** used an effective spin-1/2 Hamiltonian to avoid over parameterization. This contrasts with other studies that use more sophisticated Hamiltonians to model the Γ_8 quartet ground state of an ideal tetrahedral (T_d) crystal field.[18] This choice is justified by the lower symmetry of **1-Pr** and the energies of the ground state $^2F_{5/2}$ manifold predicted by the (SO)-XMS-CASPT2 calculations.[13] This simulation yielded the following parameters: g_z = 2.74, g_y = 1.43, g_x = 0.96, A_z = 4170 MHz, A_y = 2240 MHz, and A_x = 1720 MHz. The EPR data support the previous[2] assignment of the spectrum of **1-Pr*** as indeed originating from a Pr^{4+} complex in solution (see Fig. S24 for co-plot of **1-Pr** and **1-Pr***). The spectrum of **2-Ce^{Cs}** (Fig. S25) is similar to a previously reported[11c] spectrum of a Ce^{3+} imidophosphorane complex, with one main transition, as expected for a Kramers doublet without hyperfine coupling.

Direct-current (DC) magnetic susceptibility measurements demonstrate that the molar susceptibility (χ_M) of **1-Pr** is lower compared to isoelectronic **2-Ce^{Cs}** at all temperatures from 1.8–300 K, indicating a smaller Landé g-factor, (Fig. 2C) in agreement with the theoretical models of **1-Pr** and **2-Ce^{Cs}** (*vide supra*). The 300 K data for **2-Ce^{Cs}** (χ_MT = 0.79 emu K mol^{-1}) agrees with the free ion $4f^1$ expected value[19] of 0.80 emu K mol^{-1}, while **1-Pr** (χ_MT = 0.64 emu K mol^{-1}) is notably below the predicted value. Similarly to **2-Ce^{Cs}**, the χ_MT value of **2-Pr^{Cs}** at room temperature is in agreement with the calculated value (χ_MT = 1.58 emu K mol^{-1} vs. 1.60 emu K mol^{-1} expected). The lower χ_MT value of 0.64 emu K mol^{-1} for **1-Pr** is attributed to partial quenching of orbital angular momentum, driven by increased formal charge of Pr^{4+}, resulting in larger splitting of the crystal field.[7] The observation of reduced χ_MT for **1-Pr** vs. **2-C^{Cs}** from T = 1.8–300 K contrasts with the data reported for Pr^{4+} supported by a siloxide ligand framework in a pseudo-octahedral coordination environment (*e.g.* [Pr^{4+}(OSiPh$_3$)$_4$(MeCN)$_2$]), wherein isoelectronic Pr^{4+} and Ce^{3+} display nearly identical magnetic susceptibility data.[4b] However, it was recently reported that replacement of MeCN ligands in [Pr^{4+}(OSiPh$_3$)$_4$(MeCN)$_2$] with a substituted bipyridine chelate was reported to reduce χ_MT[4c] to values consistent with the low χ_MT values that are characteristic of solid-state Pr^{4+} complexes in cubic oxide coordination environments.[7, 17a, 20]

An *ab initio* investigation of the g-tensors was carried out for both **1-Pr** and **2-Ce^{Cs}**, using spin-orbit (SO)-XMS-CASPT2 with an active space including a single electron distributed over the 4f and 5d orbitals, denoted (1*e*, 12*o*) (Table S11). Inclusion of the 5d orbitals in the active space resulted in g-tensor values closer to experimental values for **1-Pr**, while the g-tensor values for **2-Ce^{Cs}** were rather insensitive to inclusion of the 5d orbitals (Table S11). Calculated values for **1-Pr** were in agreement with those derived from EPR, with g_z = 2.52(2.74 exp.), and g_y = 1.26(1.43 exp.), and g_x = 0.69(0.96 exp.), supporting the theoretical model.

The crystal field splitting in the Ce^{3+} and Pr^{4+} systems was evaluated with (SO)-XMS-CASPT2,[13b] as the effectively low site symmetry of the ions preclude a physically meaningful fit to a cubic Hamiltonian.[18] In the case of **1-Pr**, the energy levels arising from the 4f-4f transitions span 141 to 4905 cm^{-1} cm^{-1}, but spans up to 2719 cm^{-1} for **2-Ce^{Cs}**. We note that the energy range of the 4f-4f excitations slightly varies depending on the choice of active space, (i.e., with or without 5d orbitals, Table S8, S9), but remain consistent with the larger crystal-field splitting of the 4f orbitals in **1-Pr**. Furthermore, the calculated relative energy separation between the states originating from the lowest energy 4f orbital and the lowest 5d orbitals of **2-Ce^{Cs}** is 29,500 cm^{-1}. This result is in good agreement with the UV-vis spectrum, which shows a 4f-5d transition at 26,700 cm^{-1}.

While 4f covalency is increased in the Ln^{4+} oxidation state versus Ln^{3+},[7, 14a, 14c, 16, 21] the crystal field splitting of the 4f orbitals is demonstrated to be higher in **1-Pr** than in the isoelectronic $4f^1$ congener, **2-Ce^{Cs}**. The effect of the increased charge of the ion is apparent even in these 4-coordinate complexes, where a lower crystal field is expected due to a reduced number of donors, *inter alia*, compared to cubic oxide supported ions.[7, 17a, 20] This lower coordinate complex, **1-Pr**, demonstrates the utility of coordination

chemistry in tuning the crystal field experienced by Pr^{4+} and the relative quenching of orbital angular momentum.

In comparison to Ce^{3+}, the orbital angular momentum of the Pr^{4+} ion f^1 configuration is sensitive to the magnitude and symmetry of the crystal field (as determined by ligand type, coordination number, symmetry). The tetravalent oxidation state is critical: in the nearly isotypic Ce^{3+} and Pr^{4+} complexes examined here, Ce^{3+} exhibits free-ion magnetic behavior. Specifically, the $\chi_M T$ value observed for **1-Pr** is slightly lower than that of **2-Ce^{Cs}** at all temperatures, which is consistent with *g* values determined by EPR and computational analysis. This decrease in *g* is attributed to partial quenching of orbital angular momentum at Pr^{4+} in **1-Pr** in comparison to Ce^{3+} in **2-Ce^{Cs}**, which is expected as the crystal field strength increases. As the crystal field increases at Pr^{4+}, competition between crystal field and SOC grows, and the Pr^{4+} single-ion properties can resemble those of high-valent actinides.[7, 22] The unique susceptibility of **1-Pr**, in between that of solid-state oxides and other molecular examples, demonstrates the tuning of the magnetic properties of Ln^{4+} systems by modification of the coordination environment. Direct measurement of the crystal field transitions via inelastic neutron scattering and far-infrared magnetospectroscopy (FIRMS) studies will further delineate the magnitude of the pseudo-tetrahedral crystal field at molecular Pr^{4+} and the competing interactions driving the deviation from the idealized Γ_8 ground state.

Supporting Information

The authors have cited additional references within the Supporting Information.[23-43]

Acknowledgements

The experimental work was supported by a National Science Foundation (NSF) CAREER grant under award no. 1943452 (ACB, HSL). HSL is an Alfred P. Sloan Research Fellow. The computational work was supported by the U.S. Department of Energy, Office of Science, Office of Basic Energy Sciences, Heavy Element Chemistry Program, under Award Number DESC0023022 (SRC, BV). Computations supporting this project were performed on high-performance computing systems at the University of South Dakota, funded by NSF award OAC1626516 (SRC, BV). BV and SRC acknowledge that the land this research was performed on is the original homeland of the Dakota, Lakota, and Nakota tribal nations. Use of the Stanford Synchrotron Radiation Lightsource (SSRL), SLAC National Accelerator Laboratory, is supported by the U.S. Department of Energy, Office of Science, Office of Basic Energy Sciences under Contract No. DE-AC02-76SF00515. The SSRL Structural Molecular Biology Program is supported by the DOE Office of Biological and Environmental Research, and by the National Institutes of Health, National Institute of General Medical Sciences (including P30GM133894). A portion of the magnetic measurements were collected at the University of Wisconsin– Madison by Rebecca K. Walde, supported by NSF grant CHE2246913 awarded to Prof. John F. Berry. S.M.G. acknowledges support from the Laboratory Directed Research and Development program at Los Alamos National Lab (LANL) (20230399ER). LANL is managed by Triad National Security, LLC for the NNSA of the U.S. Department of Energy (contract 89233218CNA000001).

Keywords: tetravalent lanthanides • praseodymium(IV) • imidophosphoranes

References

[1] N. T. Rice, I. A. Popov, D. R. Russo, J. Bacsa, E. R. Batista, P. Yang, J. Telser, H. S. La Pierre, *J. Am. Chem. Soc.* **2019**, *141*, 13222-13233.

[2] N. T. Rice, I. A. Popov, R. K. Carlson, S. M. Greer, A. C. Boggiano, B. W. Stein, J. Bacsa, E. R. Batista, P. Yang, H. S. La Pierre, *Dalton Trans.* **2022**, *51*, 6696-6706.

[3] a) C. T. Palumbo, I. Zivkovic, R. Scopelliti, M. Mazzanti, *J. Am. Chem. Soc.* **2019**, *141*, 9827-9831; b) A. R. Willauer, C. T. Palumbo, R. Scopelliti, I. Zivkovic, I. Douair, L. Maron, M. Mazzanti, *Angew. Chem. Int. Ed.* **2020**, *59*, 3549-3553; c) T. Xue, Y.-S. Ding, X.-L. Jiang, L. Tao, J. Li, Z. Zheng, *Precis. Chem.* **2023**, *1*, 583-591; d) M. Tricoire, F.-C. Hsueh, M. Keener, T. Rajeshkumar, R. Scopelliti, I. Zivkovic, L. Maron, M. Mazzanti, *Chem. Sci.* **2024**, *15*, 6874-6883.

[4] a) A. R. Willauer, I. Douair, A.-S. Chauvin, F. Fadaei-Tirani, J.-C. G. Bünzli, L. Maron, M. Mazzanti, *Chem. Sci.* **2022**, *13*, 681-691; b) A. R. Willauer, C. T. Palumbo, F. Fadaei-Tirani, I. Zivkovic, I. Douair, L. Maron, M. Mazzanti, *J. Am. Chem. Soc.* **2020**, *142*, 5538-5542; c) T. Xue, Y. Ding, Z. Zheng, *Dalton Trans.* **2024**, *53*, 5779-5783.

[5] a) T. P. Gompa, A. Ramanathan, N. T. Rice, H. S. La Pierre, *Dalton Trans.* **2020**, *49*, 15945-15987; b) N. A. Piro, J. R. Robinson, P. J. Walsh, E. J. Schelter, *Coord. Chem. Rev.* **2014**, *260*, 21-36.

[6] A. Ramanathan, E. D. Walter, M. Mourigal, H. S. La Pierre, *J. Am. Chem. Soc.* **2023**, *145*, 17603-17612.

[7] A. Ramanathan, J. Kaplan, D.-C. Sergentu, J. A. Branson, M. Ozerov, A. I. Kolesnikov, S. G. Minasian, J. Autschbach, J. W. Freeland, Z. Jiang, M. Mourigal, H. S. La Pierre, *Nat. Commun.* **2023**, *14*, 3134.

[8] R. Shannon, *Acta Crystallogr. A* **1976**, *32*, 751-767.

[9] L. Yang, D. R. Powell, R. P. Houser, *Dalton Trans.* **2007**, 955-964.

[10] P. Å. Malmqvist, A. Rendell, B. O. Roos, *J. Phys. Chem.* **1990**, *94*, 5477-5482.

[11] a) A. C. Boggiano, C. M. Studvick, A. Steiner, J. Bacsa, I. A. Popov, H. S. La Pierre, *Chem. Sci.* **2023**, *14*, 11708-11717; b) N. T. Rice, I. A. Popov, D. R. Russo, T. P. Gompa, A. Ramanathan, J. Bacsa, E. R. Batista, P. Yang, H. S. La Pierre, *Chem. Sci.* **2020**, *11*, 6149-6159; c) N. T. Rice, J. Su, T. P. Gompa, D. R. Russo, J. Telser, L. Palatinus, J. Bacsa, P. Yang, E. R. Batista, H. S. La Pierre, *Inorg. Chem.* **2019**, *58*, 5289-5304.

[12] K. S. Otte, J. E. Niklas, C. M. Studvick, A. C. Boggiano, J. Bacsa, I. A. Popov, H. S. La Pierre, *Angew. Chem. Int. Ed.* **2023**, *62*, e202306580.

[13] a) P. Å. Malmqvist, B. O. Roos, B. Schimmelpfennig, *Chem. Phys. Lett.* **2002**, *357*, 230-240; b) A. A. Granovsky, *J. Chem. Phys.* **2011**, *134*, 214113.

[14] a) S. G. Minasian, E. R. Batista, C. H. Booth, D. L. Clark, J. M. Keith, S. A. Kozimor, W. W. Lukens, R. L. Martin, D. K. Shuh, S. C. E. Stieber, T. Tylisczcak, X.-d. Wen, *J. Am. Chem. Soc.* **2017**, *139*, 18052-18064; b) H. Dexpert, R. C. Karnatak, J. M. Esteva, J. P. Connerade, M. Gasgnier, P. E. Caro, L. Albert, *Phys. Rev. B* **1987**, *36*, 1750-1753; c) M. W. Löble, J. M. Keith, A. B. Altman, S. C. E. Stieber, E. R. Batista, K. S. Boland, S. D. Conradson, D. L. Clark, J. Lezama Pacheco, S. A. Kozimor, *J. Am. Chem. Soc.* **2015**, *137*, 2506-2523.

[15] A. Bianconi, A. Marcelli, H. Dexpert, R. Karnatak, A. Kotani, T. Jo, J. Petiau, *Phys. Rev. B* **1987**, *35*, 806-812.

[16] W. W. Lukens, S. G. Minasian, C. H. Booth, *Chem. Sci.* **2023**, *14*, 12784-12795.

[17] a) Y. Hinatsu, *J. Solid State Chem.* **1997**, *128*, 228-232; b) Y. Hinatsu, N. Edelstein, *J. Alloys Compd.* **1997**, *250*, 400-404; c) Y. Hinatsu, *J. Solid State Chem.* **1996**, *122*, 384-389; d) K. Tezuka, Y. Hinatsu, *J. Solid State Chem.* **1999**, *143*, 140-143; e) Y. Hinatsu, N. Edelstein, *J. Solid State Chem.* **1994**, *112*, 53-57.

[18] a) B. Bleaney, *Proc. Phys. Soc.* **1959**, *73*, 939; b) B. Bleaney, *Proc. Phys. Soc.* **1959**, *73*, 937.

[19] R. S. Drago, *Physical Methods for Chemists*, Surfside Scientific Publishers, **1992**.

[20] a) M. Bickel, G. L. Goodman, L. Soderholm, B. Kanellakopulos, *J. Solid State Chem.* **1988**, *76*, 178-185; b) M. J. Daum, A. Ramanathan, A. I. Kolesnikov, S. Calder, M. Mourigal, H. S. La Pierre, *Phys. Rev. B* **2021**, *103*, L121109; c) S. Kern, *J. Chem. Phys.* **1964**, *40*, 208-212; d) J. B. MacChesney, H. J. Williams, R. C. Sherwood, J. F. Potter, *J. Chem. Phys.* **1964**, *41*, 3177-3178.

[21] T. P. Gompa, S. M. Greer, N. T. Rice, N. Jiang, J. Telser, A. Ozarowski, B. W. Stein, H. S. La Pierre, *Inorg. Chem.* **2021**, *60*, 9064-9073.

[22] a) M. Gregson, E. Lu, D. P. Mills, F. Tuna, E. J. L. McInnes, C. Hennig, A. C. Scheinost, J. McMaster, W. Lewis, A. J. Blake, A. Kerridge, S. T. Liddle, *Nat. Commun.* **2017**, *8*, 14137; b) W. W. Lukens, N. M. Edelstein, N. Magnani, T. W. Hayton, S. Fortier, L. A. Seaman, *J. Am. Chem. Soc.* **2013**, *135*, 10742-10754; c) J. A. Seed, L. Birnoschi, E. Lu, F. Tuna, A. J. Wooles, N. F. Chilton, S. T. Liddle, *Chem* **2021**, *7*, 1666-1680; d) J. C. Eisenstein, M. H. L. Pryce, *Proc. R. Soc. Lond. A* **1997**, *255*, 181-198; e) N. M. Edelstein, G. H. Lander, in *The Chemistry of the Actinide and Transactinide Elements* (Eds.: L. R. Morss, N. M. Edelstein, J. Fuger), Springer Netherlands, Dordrecht, **2011**, pp. 2225-2306.

[23] S. A. Johnson, J. J. Kiernicki, P. E. Fanwick, S. C. Bart, *Organometallics* **2015**, *34*, 2889-2895.

[24] H. Tateyama, A. C. Boggiano, C. Liao, K. S. Otte, X. Li, H. S. La Pierre, *J. Am. Chem. Soc.* **2024**, *146*, 10268-10273.

[25] B. Ravel, M. Newville, *J. Synchrotron Rad.* **2005**, *12*, 537-541.

[26] M. Newville, R. Otten, A. Nelson, T. Stensitzki, A. Ingargiola, D. Allan, A. Fox, F. Carter, Michal, R. Osborn, D. Pustakhod, Ineuhaus, S. Weigand, A. Aristov, Glenn, C. Deil, mgunyho, Mark, A. L. R. Hansen, G. Pasquevich, L. Foks, N. Zobrist, O. Frost, Steurmer, azelcer, A. Polloreno, A. Persaud, J. Hedegaard Nielsen, M. Pompili, P. Eendebak*, Vol. 1.2.2*, Zenodo, **2023**.

[27] R. L. Halbach, G. Nocton, C. H. Booth, L. Maron, R. A. Andersen, *Inorg. Chem.* **2018**, *57*, 7290-7298.

[28] a) C. H. Booth, M. D. Walter, M. Daniel, W. W. Lukens, R. A. Andersen, *Phys. Rev. Lett.* **2005**, *95*, 267202; b) M. D. Walter, C. H. Booth, W. W. Lukens, R. A. Andersen, *Organometallics* **2009**, *28*, 698-707.

[29] G. A. Bain, J. F. Berry, *J. Chem. Educ.* **2008**, *85*, 532.

[30] O. Kahn, *Molecular Magnetism*, Dover Publications, **2021**.

[31] V8.40B ed., Bruker, Madison, WI, USA.

[32] L. Krause, R. Herbst-Irmer, G. M. Sheldrick, D. Stalke, *J. Appl. Crystallogr.* **2015**, *48*, 3-10.

[33] G. Sheldrick, *Acta Crystallogr. C* **2015**, *71*, 3-8.

[34] O. V. Dolomanov, L. J. Bourhis, R. J. Gildea, J. A. K. Howard, H. Puschmann, *J. Appl. Crystallogr.* **2009**, *42*, 339-341.

[35] B. O. Roos, P. R. Taylor, P. E. M. Sigbahn, *Chem. Phys.* **1980**, *48*, 157-173.

[36] B. A. Hess, *Phys. Rev. A* **1986**, *33*, 3742-3748.

[37] B. O. Roos, R. Lindh, P.-Å. Malmqvist, V. Veryazov, P.-O. Widmark, A. C. Borin, *J. Phys. Chem. A* **2008**, *112*, 11431-11435.

[38] F. Aquilante, P.-Å. Malmqvist, T. B. Pedersen, A. Ghosh, B. O. Roos, *J. Chem. Theory Comput.* **2008**, *4*, 694-702.

[39] L. F. Chibotaru, L. Ungur, *J. Chem. Phys.* **2012**, *137*, 064112.

[40] G. Li Manni, R. K. Carlson, S. Luo, D. Ma, J. Olsen, D. G. Truhlar, L. Gagliardi, *J. Chem. Theory Comput.* **2014**, *10*, 3669-3680.

[41] J. J. Bao, C. Zhou, Z. Varga, S. Kanchanakungwankul, L. Gagliardi, D. G. Truhlar, *Faraday Discuss.* **2020**, *224*, 348-372.

[42] V. Sauri, L. Serrano-Andrés, A. R. M. Shahi, L. Gagliardi, S. Vancoillie, K. Pierloot, *J. Chem. Theory Comput.* **2011**, *7*, 153-168.

[43] G. Li Manni, I. Fdez. Galván, A. Alavi, F. Aleotti, F. Aquilante, J. Autschbach, D. Avagliano, A. Baiardi, J. J. Bao, S. Battaglia, L. Birnoschi, A. Blanco-González, S. I. Bokarev, R. Broer, R. Cacciari, P. B. Calio, R. K. Carlson, R. Carvalho Couto, L. Cerdán, L. F. Chibotaru, N. F. Chilton, J. R. Church, I. Conti, S. Coriani, J. Cuéllar-Zuquin, R. E. Daoud, N. Dattani, P. Decleva, C. de Graaf, M. G. Delcey, L. De Vico, W. Dobrautz, S. S. Dong, R. Feng, N. Ferré, M. Filatov, L. Gagliardi, M. Garavelli, L. González, Y. Guan, M. Guo, M. R. Hennefarth, M. R. Hermes, C. E. Hoyer, M. Huix-Rotllant, V. K. Jaiswal, A. Kaiser, D. S. Kaliakin, M. Khamesian, D. S. King, V. Kochetov, M. Krośnicki, A. A. Kumaar, E. D. Larsson, S. Lehtola, M.-B. Lepetit, H. Lischka, P. López Ríos, M. Lundberg, D. Ma, S. Mai, P. Marquetand, I. C. D. Merritt, F. Montorsi, M. Mörchen, A. Nenov, V. H. A. Nguyen, Y. Nishimoto, M. S. Oakley, M. Olivucci, M. Oppel, D. Padula, R. Pandharkar, Q. M. Phung, F. Plasser, G. Raggi, E. Rebolini, M. Reiher, I. Rivalta, D. Roca-Sanjuán, T. Romig, A. A. Safari, A. Sánchez-Mansilla, A. M. Sand, I. Schapiro, T. R. Scott, J. Segarra-Martí, F. Segatta, D.-C. Sergentu, P. Sharma, R. Shepard, Y. Shu, J. K. Staab, T. P. Straatsma, L. K. Sørensen, B. N. C. Tenorio, D. G. Truhlar, L. Ungur, M. Vacher, V. Veryazov, et al., *J. Chem. Theory Comput.* **2023**, *19*, 6933-6991.

Table of Contents

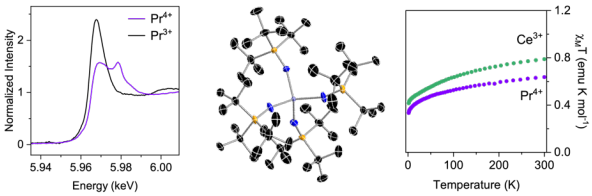

A crystallographically characterized Pr^{4+} imidophosphorane complex of is presented, $[Pr^{4+}(NP^tBu_3)_4]$ (where ^tBu = $C(CH_3)_3$), which exhibits a pseudo-tetrahedral coordination geometry in the solid state. The complex exhibits remarkable thermal stability, facilitating rigorous physical characterization that demonstrates the isoelectronic Ce^{3+} and Pr^{4+} ions exhibit divergent magnetic properties.